PCCP

Accepted Manuscript

ROYAL SOCIETY OF CHEMISTRY

www.rsc.org/pccp

PCCP

RSCPublishing

ARTICLE

Two-dimensional Raman correlation spectroscopy reveals molecular structural changes during temperature-induced self-healing in polymers based on the Diels-Alder reaction

Cite this: DOI: 10.1039/x0xx00000x

Received 00th January 2012,
Accepted 00th January 2012

DOI: 10.1039/x0xx00000x

www.rsc.org/

R. Geitner[a], J. Kötteritzsch[b,c], M. Siegmann[a], T. W. Bocklitz[a], M. D. Hager[b,c], U. S. Schubert[b,c], S. Gräfe[a], B. Dietzek[a,c,d], M. Schmitt[a] and J. Popp[a,c,d]

The thermally healable polymer P(LMA-*co*-FMA-*co*-MIMA) has been studied by temperature-dependent FT-Raman spectroscopy, two-dimensional Raman correlation analysis and density functional theory (DFT) calculations. To the best of our knowledge this study reports for the first time on the investigation of a self-healing polymer by means of two-dimensional correlation techniques. The synchronous correlation spectrum reveals that the spectrally overlapping C=C stretching vibrations at 1501, 1575, 1585 and 1600 cm^{-1} are perfect marker bands to monitor the healing process which is based on a Diels-Alder reaction of furan and maleimide. The comparison between experimental and calculated Raman spectra as well as their correlation spectra showed a good agreement between experiment and theory. The data presented within this study nicely demonstrate that Raman correlation analysis combined with a band assignment based on DFT calculations presents a powerful tool to study the healing process of self-healing polymers.

1. Introduction

Self-healing polymers represent a new material class offering the opportunity to severely increase the lifetime of materials. The self-healing property is often based on reversible chemical reactions like Diels-Alder reactions[1-6], or reversible supramolecular interactions, like hydrogen bonds[7,8], ionic interactions[9,10] or metal-ligand interactions[11-15]. All systems utilize the fact that these chemical reactions and interactions, respectively, allow – upon induction of a mobile phase, *e.g.*, by temperature treatment – (re)flow of material into the damage site and subsequently linking this phase to the polymer network to restore the original material properties. Depending on the nature of the underlying healing reaction the recovery of the initial properties can be achieved autonomously or by means of external stimuli.

The Diels-Alder reaction is a highly versatile, customizable and reversible [4+2]-cycloaddition[16,17], which features a dynamic equilibrium between the Diels-Alder and the retro Diels-Alder reaction. At lower temperatures the Diels-Alder reaction forms a six-membered ring due to the reaction of a diene and dienophile. Consequently, at higher temperatures the equilibrium is reversed and the retro Diels-Alder reaction leads to a splitting of the six-membered ring back into the diene and the dienophile. The adjustability and the aforementioned reversibility make the Diels-Alder reaction an ideal candidate for being implemented into self-healing polymers.

[a] *Institute for Physical Chemistry and Abbe Center of Photonics, Friedrich Schiller University Jena, Helmholtzweg 4, 07743, Jena, Germany.*
[b] *Laboratory for Organic and Macromolecular Chemistry (IOMC), Friedrich Schiller University Jena, Humboldtstr. 10, 07743, Jena, Germany*
[c] *Jena Center of Soft Matter (JCSM), Friedrich Schiller University Jena, Philosophenweg 7,07743, Jena, Germany*
[d] *Leibniz Institute for Photonic Technology (IPHT) Jena, Albert-Einstein-Str. 9, 07745, Jena, Germany. E-mail: juergen.popp@uni-jena.de*
Electronic Supplementary Information (ESI) available: See DOI: 10.1039/b000000x/

With this in mind it comes as no surprise that a large amount of self-healing polymers based on the Diels-Alder reaction are reported.[1-5,18,19] The [4+2]-cycloaddition is used in different approaches to introduce the self-healing function into polymers. Early approaches incorporated the diene or dienophile into the polymer molecules and used multifunctional small molecules to crosslink the strands.[1,3,5,20] Recently, the attention shifted to polymers where diene and dienophile are covalently integrated into the same polymer (one-component-system). Kötteritzsch *et al*. have synthesized a polymer based on methacrylate bearing furan and maleimide functionalities (see figure 1).[4] They used lauryl methacrylate (LMA) to introduce the necessary mobility into the polymer allowing self-healing to take place.

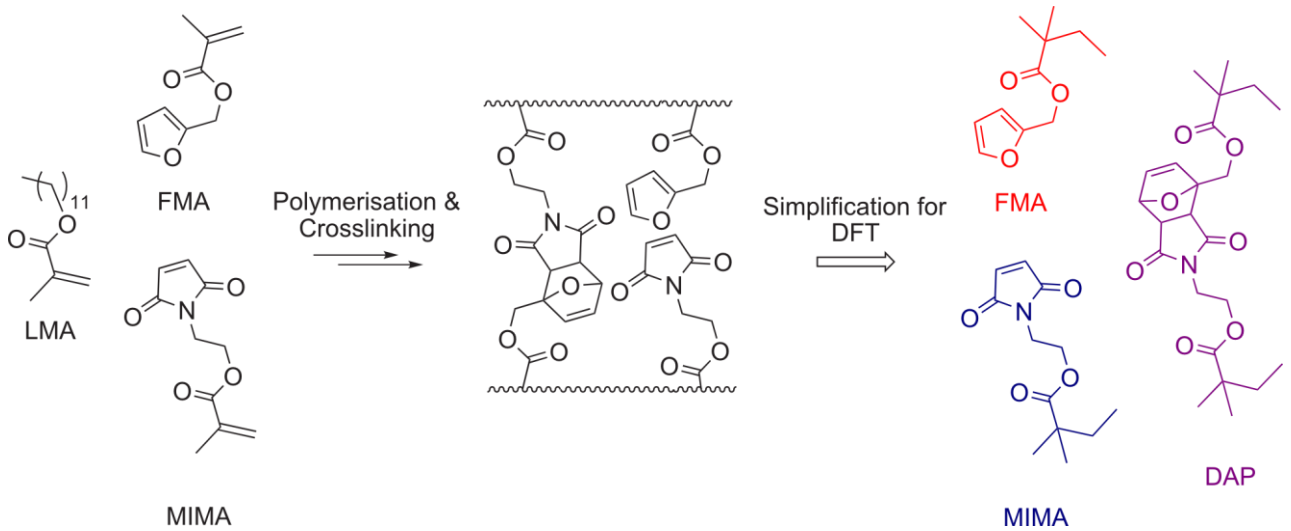

Figure 1 The monomers furfuryl methacrylate (FMA), maleimide methacrylate (MIMA) (furan-protected MIMA was used in the polymer synthesis, for details see text) and lauryl methacrylate (LMA) (left side) used in the polymerisation to build the copolymer P(LMA-*co*-FMA-*co*-MIMA) with monomer ratios of 1:1:1 (**P1**) and 8:1:1 (**P2**). For the DFT calculations simplified structures have been used (right side).

To analyse the chemical mechanisms involved in self-healing and to improve self-healing materials in detail, spectroscopic studies on self-healing polymers are important.[2,15,21-24] In this context vibrational spectroscopy such as, *e.g.*, Raman spectroscopy is especially noteworthy since the probing of molecular vibrations grants direct insight into the molecular reactions taking place during the macroscopic self-healing process.[15,22] Kupfer *et al*. used a combination of resonance Raman measurements and density functional theory (DFT) calculations to unveil the mechanisms involved in the self-healing of supramolecular polymers.[15] Bose *et al*. performed a combined Fourier transform infrared (FT IR) and oscillatory shear rheological study on Diels-Alder based polymers to link molecular reversibility and macroscale healing.[2] Harrington *et al*. applied strain-dependent Raman spectroscopy to investigate reversible protein backbone conformation changes in whelk egg capsules of *Busycotypus canaliculatus*.[24]

However, the application of vibrational spectroscopy to study chemical reactions initiated by a stimulus like, *e.g.*, temperature relies on an appropriate spectral analysis to qualitatively and quantitatively interpret the changes observed in a vibrational spectrum. In this context two-dimensional correlation spectroscopy (2D correlation spectroscopy) first introduced by Noda in 1986[25,26] and later generalized in 1993[27] is a powerful analysis approach to emphasize specific spectroscopic information from a dataset by spreading the spectral information over two dimensions. The different correlation analysis methods are described in an excellent manner by Noda.[26-30] Briefly, an external perturbation, *e.g.*, time, temperature or stress is applied to a sample which is then studied by spectroscopy. The perturbation-dependent spectral dataset is then analysed by the correlation procedure either based on the Fourier- or the Hilbert-Noda-transformation. The correlation analysis emphasizes the deviation of spectra from a predefined reference state. The results of the two-dimensional correlation analysis are the so called synchronous and asynchronous correlation spectra. The synchronous spectrum holds information about which spectral features change "in-phase", while the asynchronous spectrum shows which changes take place "out-of-phase". To interpret the signals in 2D correlation spectra the Noda rules are commonly applied, which are excellently described elsewhere.[31]

Two-dimensional correlation analysis has been successfully applied to interpret perturbation-dependent Raman spectra of polymers.[32-38] Sinzawa *et al*. for example studied the pre-melting behaviour of polyethylene between 30 and 100 °C with 2D correlation Raman spectroscopy.[39] Another study by Brewster *et al*. used 2D Raman correlation analysis to unveil structural changes in ribonuclease proteins induced by different guanidine hydrochloride concentrations between 0 and 6 M.[40]

To the best of our knowledge 2D correlation Raman spectroscopy has so far never been used to study self-healing polymers. Here we apply 2D correlation analysis on temperature-dependent Fourier transform Raman spectra (FT Raman spectra) of two furan-maleimide based self-healing polymers. This 2D correlation Raman spectroscopic approach offers the opportunity to better understand and characterize the self-healing process. Furthermore, to assist the molecular interpretation of the 2D analysis, DFT calculations have been utilized. By comparing the experimental and calculated Raman spectra and their 2D correlation spectra, the spectral regions that are specific for the self-healing Diels-Alder reaction could be identified and interpreted with respect to the underlying molecular changes which are prevalent during the self-healing process.

2. Methods

2.1 Polymer synthesis

The synthesis of the monomer maleimide methacrylate (MIMA) (see Figure 1) was performed like described in the literature.[4] The synthesis of the copolymer P(LMA-*co*-FMA-*co*-MIMA) with monomer ratios of 1:1:1 (**P1**) and P(MIMA) were adapted from literature reports.[4] The copolymer P(LMA-*co*-FMA-*co*-MIMA) with monomer ratios of 8:1:1 (**P2**) was also synthesized as described in literature.[4]

2.2 FT-Raman measurements

Temperature-dependent FT-Raman spectra were recorded up to 3600 cm^{-1} with a spectral resolution of 4 cm^{-1} using a commercial Bruker MultiSpec spectrometer. The Raman excitation light at 1064 nm was provided by a Nd:YAG laser (Klastech DeniCAFC-LC-3/40). The laser power at the sample was 210 mW for **P1** and

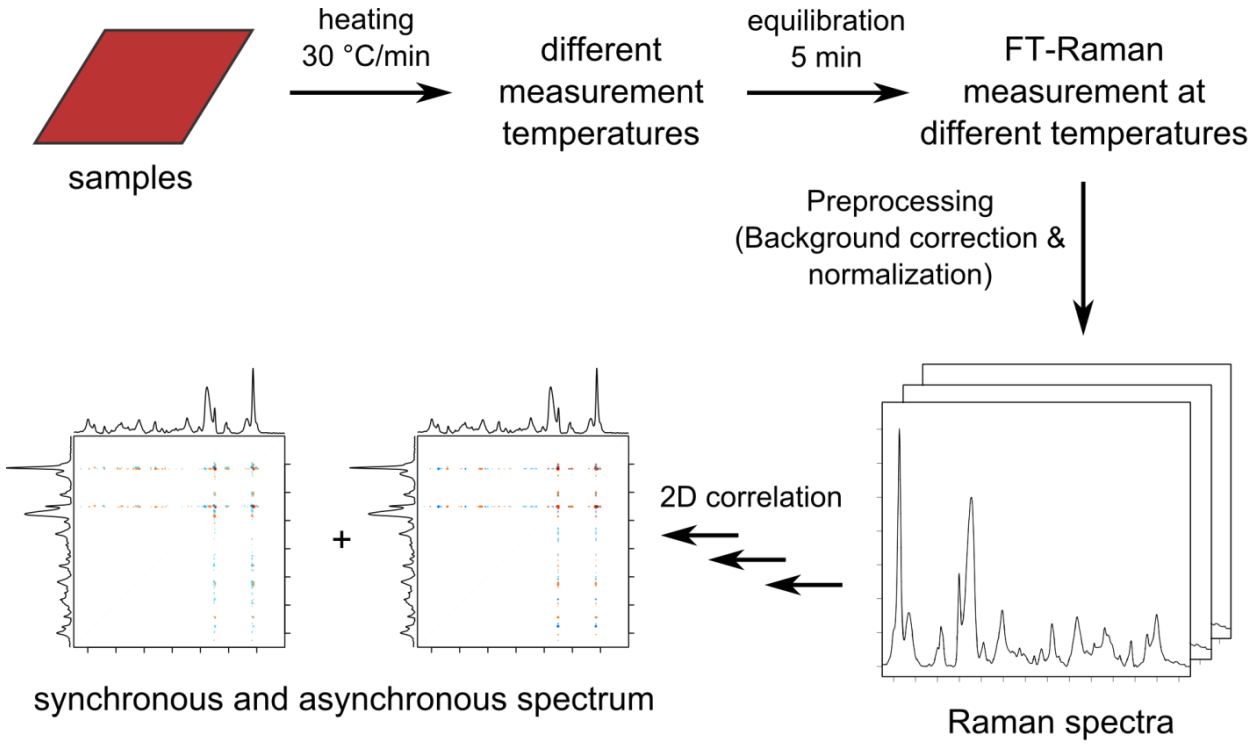

Figure 2 Flowchart for the experimental procedure to study the copolymer P(LMA-*co*-FMA-*co*-MIMA) with monomer ratios of 1:1:1 (**P1**) and 8:1:1 (**P2**).

400 mW for **P2**. The Raman spectra were recorded using the software package OPUS 6.5. The sample temperature was adjusted via a Linkam stage LTS 350. The polymer samples were first heated to 160 °C for 3 hours to remove the furan protecting group of the MIMA, which was utilized to prevent crosslinking during polymerization and were then allowed to cool down to 40 °C over night to allow the Diels-Alder mediated crosslinking to take place.

For every sample 72 (**P1**) or 178 (**P2**) Raman spectra were recorded at room temperature to confirm whether the crosslinking took place. Afterwards, the samples were heated to the different measurement temperatures (110, 120, 130, 140, 150 and 160 °C for **P1** or 110, 120, 130, 140 and 150 °C for **P2**) at a constant rate of 30 °C/min. For every temperature, a new sample was used to eliminate possible changes due to the second heating cycle. In total 6 (**P1**) and 5 (**P2**) samples were measured, respectively. The samples were allowed to equilibrate for 5 minutes at the respective measurement temperature before the Raman measurement was started. After the Raman measurement, the sample was cooled to room temperature (using liquid nitrogen at the Linkam stage) and measured again to check if the heating or the laser power damaged it. For **P1** a total of 2520 Raman spectra were recorded over 70 minutes while for **P2** a total of 1440 Raman spectra were recorded over 40 minutes for every temperature. The Raman spectra showed no spectral changes over the measurement time. For the band assignment, the Raman spectra of the monomers FMA and of furan protected MIMA and of furan protected P(MIMA) (see supporting information figure S1, S2 and S3) were also measured.

2.3 Data pre-processing

The raw Raman spectra were pre-processed using R (3.1.2).[41] First all Raman spectra recorded for one specific temperature were summed up to increase the signal-to-noise ratio. Afterwards the Raman spectra were restricted to the wavenumber region of interest, *i.e.*, the region between 180 and 2000 cm^{-1} to reduce the computational demand of the following correlation analysis. Subsequently, the Raman data were background corrected using a SNIP algorithm (iterations = 85, order = 2, smoothing window = 3) and normalized to the Raman peak at 1446 cm^{-1}, which can be assigned to CH-wagging vibrations of the polymers. It is reasonable to assume that the heating and the observed Diels-Alder reaction do not influence the intensity of these CH-wagging vibrations. The temperature-dependent FT-Raman spectra were 2D correlated using a self-written R-script based on the Fourier-transform approach. The spectrum at the lowest temperature (110 or 120 °C, respectively) was used as reference. The 2D correlation Raman spectra were created by an arbitrary selection of the contour levels. The contour levels around 0 were omitted because they only contain noise contributions, thus only the highest peaks in the selected spectral regions are shown.
Figure 2 summarizes the experimental procedure described in the paragraphs 2.2 and 2.3.

2.4 Density functional theory calculations

To further investigate the self-healing mechanism for the present class of polymers, quantum chemical calculations were performed. In order to reduce the computational demand, only the monomers MIMA and FMA as well as the respective exo- and endo-Diels-Alders products (exo- and endo-DAP) were considered (see Figure 1). Because the incorporation of the monomers into the polymer backbone occurred at the terminal ethyl moieties of the monomers, these moieties were replaced by propyl groups to better mimic the structure in the self-healing polymer (see Figure 1). All quantum chemical simulations were performed at the DFT level of theory with the global hybrid functional B3LYP[42,43] and the 6-311+G(d,p) triple-ζ basis set[44,45] implemented in the Gaussian 09 program[46]. The fully relaxed equilibrium structures of simulated MIMA, FMA, and

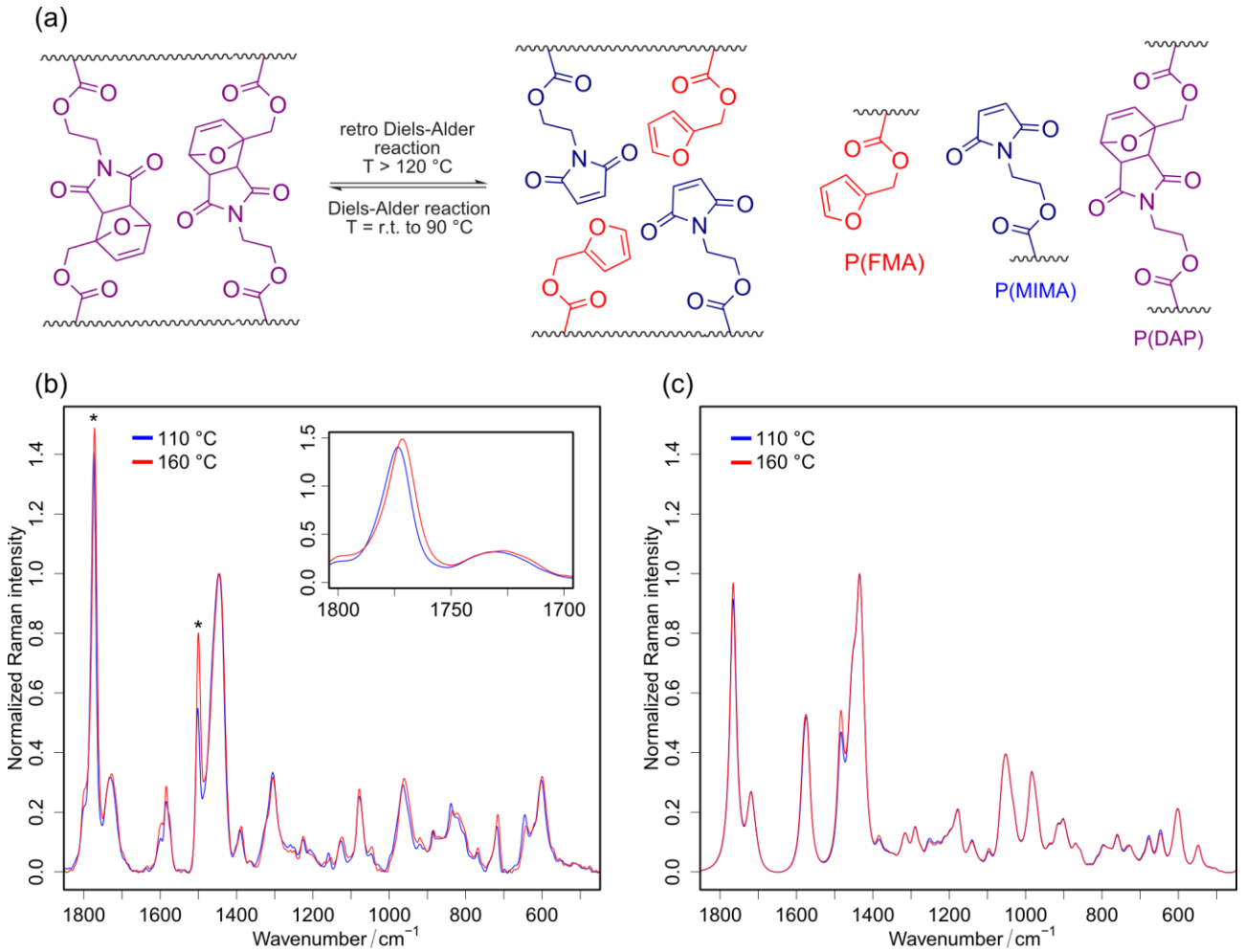

Figure 3 (a) Reaction scheme for the (retro) Diels-Alder reaction taking place in the self-healing polymers **P1** and **P2**: The maleimide and furan groups of P(MIMA) and P(FMA) (MIMA and FMA moieties in polymer, only assigned individually for better understanding) crosslink and decrosslink the polymer backbones forming DAP (Diels-Alder product of P(MIMA) and P(FMA)) depending on the temperature. (b) Experimental temperature-dependent FT-Raman spectra of **P1** for 110 °C (blue) and 160 °C (red). The Raman spectra are normalized to the Raman peak at 1446 cm^{-1}. The star (*) indicates the peaks at 1501 cm^{-1} and 1774 cm^{-1}. The inset shows the spectral region at 1700 – 1800 cm^{-1}. The Raman peak at 1774 cm^{-1} shifts slightly to lower wavenumbers for higher temperatures. (c) Corresponding simulated temperature-dependent DFT calculated Raman spectra for 110 °C (blue) and 160 °C (red). The spectra are normalized to the Raman peak at 1437 cm^{-1}. For details on the calculations see text.

their endo- and exo-DAP (see Figure 1) were obtained, while subsequent vibrational analyses determined minima of the *3N-6* dimensional potential energy (hyper-)surfaces as well as vibrational frequencies and Raman intensities. In order to account for anharmonicity and a lack of electronic correlation, the frequencies were scaled by a factor of 0.964.[47,48]

3. Results

3.1 Temperature-dependent Raman spectra

In Figure 3a the Diels-Alder reaction scheme is displayed. At lower temperatures the Diels-Alder reaction is favoured and the polymer strands are crosslinked by the P(FMA) and P(MIMA) moieties (left-hand side in Figure 3a). When the polymer is heated, the retro Diels-Alder reaction takes place. The six-membered ring in P(DAP) gets cleaved and the P(FMA) and P(MIMA) groups do not crosslink the polymer backbones any longer (right-hand side in Figure 3a). Hence the mobility of the polymers is increased and the macromolecules can now move into the damaged site to fill it. If the polymer is subsequently cooled down, the Diels-Alder reaction will take place once again and the polymer strands are bound once more *via* the P(FMA) and P(MIMA) groups. This mechanism allows the polymer to heal itself. In the following, Raman spectroscopic results are presented which allow us to follow this chemical reaction and thereby reveal molecular details.

We first study **P1** where the monomer ratio is 1:1:1 for FMA, MIMA and LMA (see Figure 1) in order to obtain higher Raman intensities for the interesting functional groups taking part in the self-healing (retro) Diels-Alder reaction. While **P1** contains all functionalities of a self-healing polymer, its self-healing capabilities have not been studied yet. However, it probably does not show any self-healing capability due to the high content of the functional monomers. Nevertheless, the results obtained from **P1** can be used to understand the spectroscopic signatures reflecting the self-healing process based on maleimide-furan Diels-Alder reactions. Afterwards, we study the polymer **P2**, which shows self-healing capabilities[2,4]. For **P2** the monomer ratio is 1:1:8 for FMA,

Table 1 Experimental and calculated wavenumbers together with their assignments for the temperature-dependent Raman bands of **P1**. Bold numbers indicate bands increasing in intensity, while normal numbers show decreasing ones with respect to the band at 1501 cm^{-1} (italic).

Exper.	Calc.	Assignment
1795		P(MIMA)[52]
1774	1765	ν_s(C=O) P(MIMA)[51,52]
1719	1709	ν_{as}(C=O) P(MIMA)[51,52]
1600	1580	ν(C=C) P(FMA)[49,50]
1585	1582	ν(C=C) P(MIMA)[52,53]
1575	1570	ν(C=C) P(DAP)
1501	1485	ν(C=C) P(FMA)[49,50]
1439		
1386	1384	ν(C-N)[54]
1302		
1258	1249	δ(C-H) P(DAP)
1148	1097	ν(C-N-C)[52,53]
1123		
1084	1058	ν(ring) P(FMA)[49]
1048	1013	δ(C-H) P(MIMA)[52,53]
980		
957	936	skeletal mode ρ(C-H) P(FMA)[49]
944	899	skeletal mode ρ(C-H) P(FMA)[49]
930	872	skeletal mode ρ(C-H) P(FMA)[49]
922	869	skeletal mode ρ(C-H) P(FMA)[49]
881	848	τ(C-H) P(FMA)[49]
842		
826	791	τ(C-H) P(FMA)[54]
811	813	τ(C-N-C)[52]
795		
766	736	ν(ring) P(MIMA)[53]
715	723	ν(ring) P(MIMA)[53]
649	645	τ(C-N-C) P(DAP)[52]
590		

MIMA and LMA. Due to the low amount of crosslinking groups in **P2** their contribution to the Raman spectra is also lower when compared to **P1** and thus it is harder to detect the changes taking place at elevated temperatures.

In Figure 3b the Raman spectra of **P1** for 110 °C and 160 °C are shown. The observed spectral changes between the two different temperatures are very subtle. Most notably the Raman bands at 1501 cm^{-1} and 1774 cm^{-1} (see * in Figure 3b) increase in intensity for higher temperatures. The Raman band at 1774 cm^{-1} also shifts 2 cm^{-1} to lower wavenumbers (see inset Figure 3b). This shift is below the spectral resolution of the FT-Raman spectra, but it is still possible to extract the information of such a sub-spectral resolution shift by applying statistical analysis. By correlating the band changes with an external parameter (like in our case the temperature) additional information is combined with the Raman spectra allowing for the extraction of sub-spectral resolution information (see section 3.4).

It should be noted that the Raman spectra at 110 °C and 120 °C do not differ from those at room temperature (see supporting information Figure S4). The band at 1501 cm^{-1} is also visible at room temperature. This band stems from the C=C stretching vibration of the furan ring in P(FMA)[49,50], showing that not all maleimide and furan groups take part in the crosslinking of the polymer at room temperature, otherwise the band at 1501 cm^{-1} belonging to the furan ring in P(FMA) would not be visible. An explanation for this behaviour is that **P1** contains a high amount of P(FMA) and P(MIMA) moieties and that not every group can find a reaction partner for the Diels-Alder reaction, because some groups are buried in the polymer coils and cannot move through the polymer to find a reaction partner.

3.2 Band assignment

In order to interpret the temperature-dependent spectral changes within the polymer **P1** it is crucial to assign the observed Raman bands to specific molecular vibrations. Table 1 summarizes all temperature-dependent Raman bands together with their assignments. The band assignments are based on Raman spectra of the monomers FMA and furan protected MIMA and furan protected P(MIMA) (see supporting information Figures S1, S2 and S3), on DFT calculations and on literature[49-54] values reported for similar systems.

3.3 Calculated Raman spectra

DFT calculations have been performed to account for the temperature-dependent changes within **P1**. The following procedure was used to simulate the temperature dependency within the polymer film: In a first step, the frequency-scaled (by a factor of 0.964) calculated Raman spectra of the products FMA and MIMA (see Figure 1) were summed up at a ratio of 1:1 to yield a combined product spectrum. In the same way, the calculated Raman spectra of exo- and endo-DAP (see Figure 1) were summed up at an arbitrary ratio of 1:1 to yield a combined educt spectrum. In order to obtain the mole fractions of the retro Diels-Alder products (FMA and MIMA) and the retro Diels-Alder educt (DAP), we have calculated the equilibrium constants K of the retro Diels-Alder reaction (see eqn. 1) for the measurement temperatures between 110 and 160 °C using the free reaction enthalpies of 8.0 kJ/mol and 15.5 kJ/mol for the endo- and exo-Diels-Alder product[55]. By using equation (2) the mole fractions of FMA and DAP were obtained. These mole fractions have been used to simulate the temperature-dependent Raman spectra of **P1** by summing up the calculated Raman spectra of the educts and products according to their respective mole fractions (see figure 3c). The spectra were normalized to the peak at 1437 cm^{-1}.

$$K = e^{-\frac{\Delta G}{RT}} \quad (1)$$

$$K = \frac{x_{FMA}^2}{x_{DAP}} \quad (2)$$

The experimental und calculated Raman spectra (see Figure 3b and 3c) match fairly well especially when considering that the LMA part of the polymer was not calculated and the ratios between the exo- and endo-Diels-Alder products are assumed arbitrarily to be 1:1.

3.4 2D Raman correlation spectra

As already mentioned, the temperature-dependent changes observed in the Raman spectra of **P1** are rather small (see Figure 3b). Thus, in order to better extract these changes and with it information on the self-healing (retro) Diels-Alder reaction, we performed a 2D correlation analysis of the temperature-dependent Raman dataset. The resultant

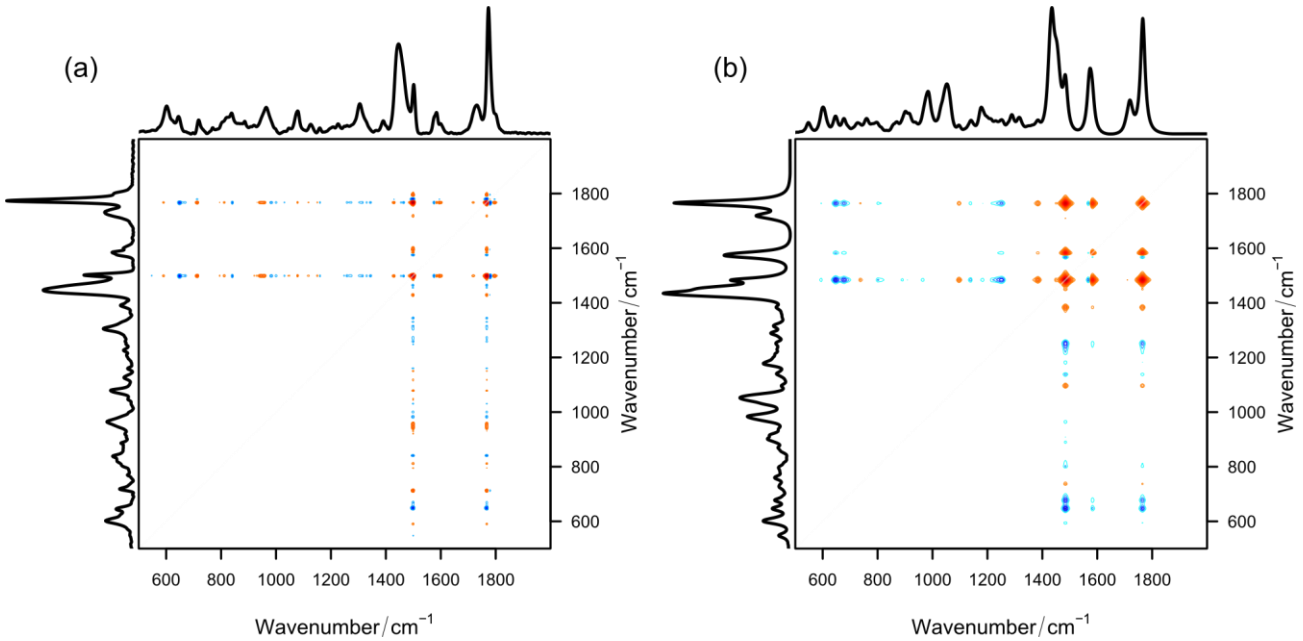

Figure 4 (a) Synchronous 2D Raman correlation spectrum of **P1** between 110 and 160 °C (in steps of 10 °C) in the wavenumber region between 500 to 2000 cm^{-1}. (b) Synchronous 2D Raman correlation spectra between 110 and 160 °C (in steps of 10 °C) in the wavenumber region between 500 to 2000 cm^{-1} as obtained from DFT calculated Raman spectra. The spectrum plotted at the top and the left is the respective reference Raman spectrum at 110 °C. Red colour indicates positive peaks, while blue shows negative ones. For details see text.

synchronous correlation spectrum is displayed in Figure 4a and selected wavenumber regions in Figure 5.

As expected from the temperature-dependent Raman spectra, the two Raman peaks at 1501 cm^{-1} and 1774 cm^{-1}, which showed the largest temperature-dependent intensity variations (see Figure 3b), exhibit the strongest auto peaks and various off-diagonal correlations, indicating that a lot of Raman peaks are influenced by the increasing temperature due to molecular changes in the polymer.

A closer look at the wavenumber region between 1700 cm^{-1} and 1850 cm^{-1} (see Figure 5) reveals that the Raman peak at 1774 cm^{-1} shows a correlation pattern consisting of two auto peaks at 1780 cm^{-1} and 1767 cm^{-1} and a negative correlation between these two. According to Czarnecki[56] such a correlation behaviour points towards a wavenumber shift, *i.e.* in our case this means that the Raman peak at 1774 cm^{-1} shifts 2 cm^{-1} to lower wavenumbers at higher temperatures resulting in the characteristic correlation pattern. This phenomenon is also observed within the temperature-dependent Raman spectra (see inset in Figure 3b). The asynchronous Raman correlation spectrum (see supporting information Figure S5) supports this finding as well. The synchronous crosspeak at 1501 cm^{-1}/1767 cm^{-1} is positive. From the Raman spectra we can see that the peak at 1501 cm^{-1} is increasing in intensity for higher temperatures. According to the Noda rules, the positive crosspeak shows that the peak at 1774 cm^{-1} is also increasing in intensity, as already deduced from the Raman spectra.

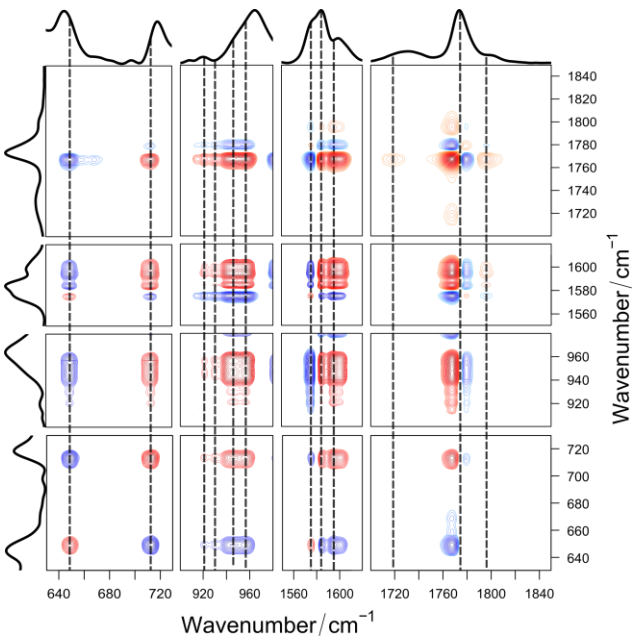

Figure 5 Selected wavenumber regions of the synchronous 2D Raman correlation spectrum of **P1**. The auto- and/or crosspeaks of the bands at 649, 715, 922, 930, 944, 980, 1575, 1585, 1600, 1719, 1774 and 1795 cm^{-1} can be identified. The band at 1774 cm^{-1} shows the characteristic pattern of a small wavenumber shift. The spectrum plotted at the top and the left is the reference Raman spectrum at 110 °C. Red colour indicates positive peaks, while blue shows negative ones. For details see text.

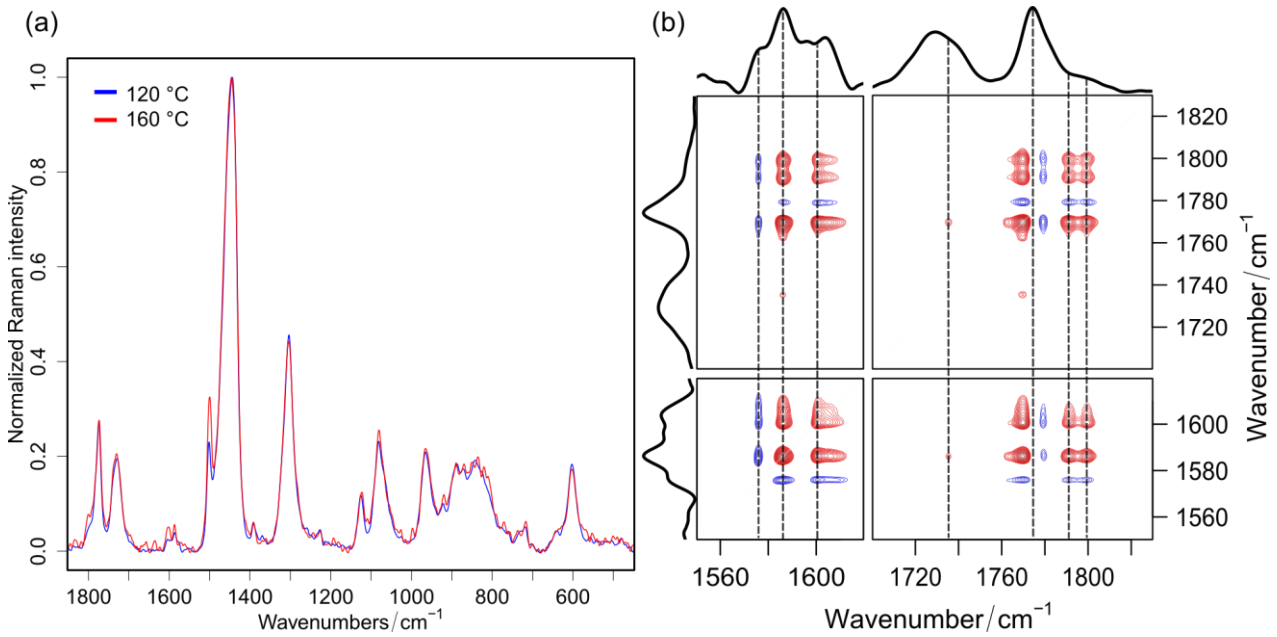

Figure 6 (a) Experimental temperature-dependent FT-Raman spectra of **P2** at 120 °C (blue) and 160 °C (red). The spectra are normalized to the peak maximum at 1446 cm^{-1}. (b) Selected regions of the synchronous 2D Raman correlation spectrum of **P2**. The auto- and/or crosspeaks of the bands at 1575, 1585, 1600, 1723, 1774, 1790 and 1799 cm^{-1} can be seen. The band at 1774 cm^{-1} shows the characteristic pattern of a small wavenumber shift. The spectrum plotted at the top and the left is the reference Raman spectrum at 120 °C. Red colour indicates positive peaks, while blue shows negative ones. For details see text.

The wavenumber region between 1550 cm^{-1} and 1620 cm^{-1} consists of strongly overlapping bands in the normal Raman spectrum that are impossible to analyse (see Figure 3b). The 2D correlation spectrum on the other hand contains three clearly resolved autopeaks at 1600 cm^{-1}, 1585 cm^{-1} and 1575 cm^{-1} (see Figure 5). All of these autopeaks show crosspeaks with each other and with the bands at 1501 cm^{-1} and 1774 cm^{-1}. The crosspeaks at 1501 cm^{-1}/1600 cm^{-1} and 1501 cm^{-1}/1585 cm^{-1} are positive, while the crosspeak at 1501 cm^{-1}/1575 cm^{-1} is negative. From this observation it can be concluded that the Raman bands at 1600 cm^{-1} and 1585 cm^{-1} are increasing and the band at 1575 cm^{-1} is decreasing in intensity upon increasing temperature. The differentiation of the three bands at 1600 cm^{-1}, 1585 cm^{-1} and 1575 cm^{-1} is only possible when using the 2D correlation analysis.

This procedure can be applied to every Raman band that shows a synchronous crosspeak with the band at 1501 cm^{-1}. All bands that show an autopeak also show a crosspeak with the band at 1501 cm^{-1}. Following this procedure the Raman bands can be divide into two groups: The Raman peaks at 1795, 1774, 1719, 1600, 1585, 1501, 1386, 1148, 1123, 1084, 1048, 957, 944, 930, 922, 881, 826, 811, 795, 766, 715 and 590 cm^{-1} are increasing in intensity, while the bands at 1575, 1439, 1386, 1302, 1258, 980, 842 and 649 cm^{-1} are decreasing in intensity for higher temperatures. Without the synchronous 2D correlation spectrum it is not possible to identify all changing Raman bands and how they change for increasing temperatures.

The simulated temperature-dependent Raman spectra (see Figure 3c) were also 2D correlated. The calculated synchronous 2D Raman spectrum can be seen in Figure 4b. The agreement between the experimental and calculated 2D correlation spectra is qualitatively excellent. While the wavenumber values are not matching exactly, the general trend is the same in both spectra. Both show the strong autopeaks at around 1500 cm^{-1} and 1780 cm^{-1}, the positive and negative correlation with the Raman bands at around 1590 cm^{-1} and the high amount of crosspeaks with the remaining bands in the fingerprint region.

In combination with the band assignment (see Table 1), the 2D synchronous correlation shows that the bands of P(DAP) (*e.g.*, 1575 and 649 cm^{-1}) decrease in intensity for higher temperatures, while the bands of P(FMA) (*e.g.*, 1600, 1501 and 1084 cm^{-1}) and P(MIMA) (*e.g.*, 1774 and 1585 cm^{-1}) increase in intensity.

Taken together the band assignments and the information from the 2D Raman spectrum show that the retro Diels-Alder reaction takes place at higher temperatures and, consequently, the polymer strands are decrosslinked (see Figure 3a right side). This proves that the Diels-Alder reaction based healing mechanism works and that the healing process can be followed by Raman spectroscopy. In particular, the four C=C vibrations at 1501 cm^{-1} and at around 1590 cm^{-1} prove to be perfectly suitable to monitor the Diels-Alder reaction.

3.4 Self-healing polymer P2

In contrast to **P1**, **P2** has already been proven to be self-healing.[2,4] We also conducted temperature-dependent Raman measurements on this polymer to characterize the self-healing process of a proven self-healing sample. The results of this study are summarized in Figure 6.

The Raman spectra (Figure 6a) look very similar to the ones of **P1** with the exception that the bands belonging to the functional groups are much lower in intensity, which can be expected since **P2** contains only one-eighth of the amount of functional groups when compared to **P1**. The three bands at around 1590 cm^{-1} and the band at 1774 cm^{-1} are much lower in intensity as compared to the Raman spectra of **P1**.

In Figure 6b two selected regions of the synchronous 2D correlation spectrum can be seen. The selected wavenumber regions and the complete 2D spectrum match well with the 2D spectrum of **P1** (see Figure 4a). Even though the

temperature-dependent spectral changes are less pronounced than in **P1**, the overall appearance of the two 2D correlation spectra is the same. For example, the wavenumber region between 1550 cm^{-1} and 1620 cm^{-1} displays again the three peaks at 1575, 1585 and 1600 cm^{-1}, while the peak at 1774 cm^{-1} shows the characteristic correlation behaviour for the small wavenumber shift. A small difference is the shoulder at 1795 cm^{-1}: It now shows two cross peaks at 1790 and 1799 cm^{-1} instead of the one at 1795 cm^{-1} in **P1**. This may be due to the smaller temperature realm over which the spectra were recorded.

Taken together, the 2D Raman correlation spectrum of **P2** is in good agreement with the expectations stemming from the observations made for **P1**. In **P2** the same bands change in intensity as in **P1**. The band assignments (see Tab. 1) of **P1** and **P2** are the same, although some temperature-dependent changes in **P2** are so small when compared to **P1** that they cannot be detected in **P2**, because the functional groups are only present "diluted" when compared to **P1**.

4. Conclusions

In this study – to the best of our knowledge – the first Raman spectroscopic 2D correlation analysis on self-healing polymers is presented. We show that this approach is promising for analysing and understanding self-healing polymers more precisely compared to using normal Raman spectroscopy by its own.

Two Diels-Alder based self-healing polymers were studied. 2D correlation allowed a correct assignment of all C=C stretching vibrations that are vital to follow the self-healing process. Furthermore, the 2D correlation offers the opportunity to study the changes of a lot of molecular vibrations simultaneously during the heating of the polymers.

In the future this technique will be applied not only to polymer systems, in which the self-healing capability is based on the Diels-Alder reaction but also to self-healing polymers using other healing processes. We are also looking into other perturbations methods, *e.g.*, stress, to study self-healing materials.

Acknowledgements

We would like to thank the Deutsche Forschungsgemeinschaft (DFG) for funding the priority program SPP 1568 "Design and Generic Principles of Self-healing Materials" and the projects PO563/25-2, DI1517/9-1 and SCHU1229/13-1 therein.

References

1 M. J. Barthel, T. Rudolph, A. Teichler, R. M. Paulus, J. Vitz, S. Hoeppener, M. D. Hager, F. H. Schacher and U. S. Schubert, *Adv. Funct. Mater.*, 2013, **23**, 4921–4932.

2 R. K. Bose, J. Kötteritzsch, S. J. Garcia, M. D. Hager, U. S. Schubert and S. van der Zwaag, *J. Polym. Sci., Part A: Polym. Chem.*, 2014, **52**, 1669–1675.

3 A. A. Kavitha and N. K. Singha, *ACS Appl. Mater. Interfaces*, 2009, **1**, 1427–1436.

4 J. Kötteritzsch, S. Stumpf, S. Hoeppener, J. Vitz, M. D. Hager and U. S. Schubert, *Macromol. Chem. Phys.*, 2013, **214**, 1636–1649.

5 C. Toncelli, De Reus, Dennis C., F. Picchioni and A. A. Broekhuis, *Macromol. Chem. Phys.*, 2012, **213**, 157–165.

6 M. D. Hager, P. Greil, C. Leyens, S. van der Zwaag and U. S. Schubert, *Adv. Mater.*, 2010, **22**, 5424–5430.

7 P. Cordier, F. Tournilhac, C. Soulié-Ziakovic and L. Leibler, *Nature*, 2008, **451**, 977–980.

8 Y. Chen, A. M. Kushner, G. A. Williams and Z. Guan, *Nature Chem.*, 2012, **4**, 467–472.

9 R. J. Varley and S. van der Zwaag, *Acta Mater.*, 2008, **56**, 5737–5750.

10 S. J. Kalista and T. C. Ward, *J. Roy. Soc. Interface*, 2007, **4**, 405–411.

11 S. Bode, R. K. Bose, S. Matthes, M. Ehrhardt, A. Seifert, F. H. Schacher, R. M. Paulus, S. Stumpf, B. Sandmann, J. Vitz, A. Winter, S. Hoeppener, S. J. Garcia, S. Spange, S. van der Zwaag, M. D. Hager and U. S. Schubert, *Polym. Chem.*, 2013, **4**, 4966–4973.

12 S. Bode, L. Zedler, F. H. Schacher, B. Dietzek, M. Schmitt, J. Popp, M. D. Hager and U. S. Schubert, *Adv. Mater.*, 2013, **25**, 1634–1638.

13 M. Burnworth, L. Tang, J. R. Kumpfer, A. J. Duncan, F. L. Beyer, G. L. Fiore, S. J. Rowan and C. Weder, *Nature*, 2011, **472**, 334–337.

14 N. Holten-Andersen, M. J. Harrington, H. Birkedal, B. P. Lee, P. B. Messersmith, K. Y. C. Lee and J. H. Waite, *P. Natl. Acad. Sci. USA*, 2011, **108**, 2651–2655.

15 S. Kupfer, L. Zedler, J. Guthmuller, S. Bode, M. D. Hager, U. S. Schubert, J. Popp, S. Gräfe and B. Dietzek, *Phys. Chem. Chem. Phys.*, 2014, **16**, 12422–12432.

16 A. Gandini, *Prog. Polym. Sci.*, 2013, **38**, 1–29.

17 H. G. O. Becker and R. Beckert, *Organikum. Organisch-chemisches Grundpraktikum*, Wiley-VCH, Weinheim, 22nd edn., 2004.

18 X. Chen, M. A. Dam, K. Ono, A. Mal, H. Shen, S. R. Nut, K. Sheran and F. Wudl, *Science*, 2002, **295**, 1698–1702.

19 J. Kötteritzsch, M. D. Hager and U. S. Schubert, *Polymer*, 2015, in press.

20 C. Zeng, H. Seino, J. Ren, K. Hatanaka and N. Yoshie, *Macromolecules*, 2013, **46**, 1794–1802.

21 J. Vega, A. Grande, S. van der Zwaag and S. Garcia, *Eur. Polym. J.*, 2014, **57**, 121–126.

22 S. Vasiliu, B. Kampe, F. Theil, B. Dietzek, D. Döhler, P. Michael, W. H. Binder and J. Popp, *Appl. Spectrosc.*, 2014, **68**, 541–548.

23 L. Zedler, M. D. Hager, U. S. Schubert, M. J. Harrington, M. Schmitt, J. Popp and B. Dietzek, *Mater. Today*, 2014, **17**, 57–69.

24 M. J. Harrington, S. S. Wasko, A. Masic, F. D. Fischer, H. S. Gupta and P. Fratzl, *J. Roy. Soc. Interface*, 2012, **9**, 2911–2922.

25 I. Noda, *Bull. Am. Phys. Soc.*, 1986, **520**.

26 I. Noda, *J. Am. Chem. Soc.*, 1989, **111**, 8116–8118.

27 I. Noda, *Appl. Spectrosc.*, 1993, **47**, 1329–1336.

28 I. Noda, *Appl. Spectrosc.*, 1990, **44**, 550–561.

29 I. Noda, *Appl. Spectrosc.*, 2000, **54**, 994–999.

30 I. Noda, *Vib. Spectrosc.*, 2012, **60**, 146–153.

31 I. Noda, *J. Mol. Struct.*, 2006, **799**, 41–47.

32 V. A. Shashilov and I. K. Lednev, *J. Raman Spectrosc.*, 2009, **40**, 1749–1758.

33 H. Tang, S. Sun, J. Wu, P. Wu and X. Wan, *Polymer*, 2010, **51**, 5482–5489.
34 L. Ashton, J. Dusting, E. Imomoh, S. Balabani and E. W. Blanch, *Biophys. J.*, 2010, **98**, 707–714.
35 L. Ashton, C. Johannessen and R. Goodacre, *Anal. Chem.*, 2011, **83**, 7978–7983.
36 V. L. Brewster, L. Ashton and R. Goodacre, *Anal. Chem.*, 2011, **83**, 6074–6081.
37 L. Ma, Z. Ahmed and S. A. Asher, *J. Phys. Chem. B*, 2011, **115**, 4251–4258.
38 V. Sikirzhytski, N. I. Topilina, G. A. Takor, S. Higashiya, J. T. Welch, V. N. Uversky and I. K. Lednev, *Biomacromolecules*, 2012, **13**, 1503–1509.
39 H. Shinzawa, Y. Ozaki and H. Chung, *Vib. Spectrosc.*, 2012, **60**, 154–157.
40 V. L. Brewster, L. Ashton and R. Goodacre, *Anal. Chem.*, 2013, **85**, 3570–3575.
41 R Core team, *R: A Language and Environment for Statistical Computing*, R Foundation for Statistical Computing, Wien, Austria, 2014.
42 A. D. Becke, *J. Chem. Phys.*, 1993, **98**, 5648–5652.
43 C. Lee, W. Yang and R. G. Parr, *Phys. Rev. B (Physical Review B)*, 1988, **37**, 785–789.
44 A. D. McLean and G. S. Chandler, *J. Chem. Phys.*, 1980, **72**, 5639–5647.
45 R. Krishnan, J. S. Binkley, R. Seeger and J. A. Pople, *J. Chem. Phys.*, 1980, **72**, 650–654.
46 M. J. Frisch, G. W. Trucks, H. B. Schlegel, G. E. Scuseria, M. A. Robb, J. R. Cheeseman, G. Scalmani, V. Barone, B. Mennucci, G. A. Petersson, H. Nakatsuji, M. Caricato, X. Li, H. P. Hratchian, A. F. Izmaylov, J. Bloino, G. Zheng, J. L. Sonnenberg, M. Hada, M. Ehara, K. Toyota, R. Fukuda, J. Hasegawa, M. Ishida, T. Nakajima, Y. Honda, O. Kitao, H. Nakai, T. Vreven, Montgomery Jr., J. A., J. E. Peralta, F. Ogliaro, M. J. Bearpark, J. Heyd, E. N. Brothers, K. N. Kudin, V. N. Staroverov, R. Kobayashi, J. Normand, K. Raghavachari, A. P. Rendell, J. C. Burant, S. S. Iyengar, J. Tomasi, M. Cossi, N. Rega, N. J. Millam, M. Klene, J. E. Knox, J. B. Cross, V. Bakken, C. Adamo, J. Jaramillo, R. Gomperts, R. E. Stratmann, O. Yazyev, A. J. Austin, R. Cammi, C. Pomelli, J. W. Ochterski, R. L. Martin, K. Morokuma, V. G. Zakrzewski, G. A. Voth, P. Salvador, J. J. Dannenberg, S. Dapprich, A. D. Daniels, Ö. Farkas, J. B. Foresman, J. V. Ortiz, J. Cioslowski and D. J. Fox, *Gaussian 09 (Revision A.02)*, Gaussian, Inc, Wallingford, CT, USA, 2009.
47 J. P. Merrick, D. Moran and L. Radom, *J. Phys. Chem. A*, 2007, **111**, 11683–11700.
48 R. D. Johnson, *NIST Standard Reference Database Number 101*, 2011.
49 L. Strandman-Long and J. Murto, *Spectrochim. Acta A-M*, 1981, **37**, 643–653.
50 C. Tarducci, J. P. S. Badyal, S. A. Brewer and C. Willis, *Chem. Commun.*, 2005, 406–408.
51 G. Socrates, *Infrared and Raman characteristic group frequencies. Tables and charts*, John Wiley & Sons, West Sussex, 3rd edn., 2007.
52 T. Woldbæk, P. Klaboe and C. Nielsen, *J. Mol. Struct.*, 1975, **27**, 283–301.
53 B. Lokshin, V. Aleksanyan, Z. Klemenkova, L. Rybin and N. Gubenko, *J. Organomet. Chem.*, 1974, **74**, 97–103.
54 C. Goussé, A. Gandini and P. Hodge, *Macromolecules*, 1998, **31**, 314–321.
55 D. Tobia, R. Harrison, B. Phillips, T. L. White, M. DiMare and B. Rickborn, *J. Org. Chem.*, 1993, **58**, 6701–6706.
56 M. A. Czarnecki, *Appl. Spectrosc.*, 1998, **52**, 1583–1590.